Determination from Space of Atmospheric Total Water Vapor Amounts by Differential Absorption near 940 nm: Theory and Airborne Verification

ROBERT FROUIN,* PIERRE-YVES DESCHAMPS** AND PIERRE LECOMTE

Laboratoire d'Optique Atmosphérique, Université des Sciences et Techniques de Lille, Lille, France

(Manuscript received 28 January 1989, in final form 30 October 1989)

ABSTRACT

A new technique is proposed to estimate atmospheric total water vapor amounts from space. The technique consists of viewing the Earth's surface in two spectral channels, one narrow, the other wide, centered on the same wavelength at the water vapor absorption maximum near 940 nm. With these characteristics, the ratio of the solar radiance measured in the two channels is independent of the surface reflectance and yields a direct estimate of the water vapor amount integrated along the optical path. To test the technique, we designed and built a two-channel radiometer based on the above concept. Airborne experiments carried out with the new device demonstrate the technique's feasibility under clear sky conditions over both sea and land. Over the ocean and in the presence of thick aerosol layers, however, total water vapor amounts may be underestimated by as much as 20%. Compared to satellite microwave techniques, which are applicable under most weather conditions, the proposed technique has the advantage of simplicity and constitutes a promising alternative over land, where microwave radiometry is inappropriate.

1. Introduction

Water vapor is an important constituent of the atmosphere. This is manifested in the ability of water vapor to change phase within atmospheric pressure and temperature ranges, producing clouds and hydrometeors (e.g., rain, snow, hail). When significant amounts of water vapor condense, the latent heat release becomes a source of energy for the maintenance of atmospheric processes. Water vapor also affects atmospheric energetics through radiative interactions.

Previous efforts to obtain water vapor data on a global scale have relied primarily upon radiosondes at hundreds of weather stations scattered around the world. Remote spectroscopy systems operating from space have more recently been deployed, and their major advantage is in obtaining continuous spatial and temporal data from not easily accessible regions (e.g., over the oceans, deserts, and poles).

Microwave measurements near the peak of the 22.235 GHz resonance line from the Nimbus series and Seasat have proved very suitable to derive the vertically integrated (or total) water vapor amount over the oceans under most atmospheric conditions (e.g., Staelin et al. 1976; Chang and Wilheit 1979; Grody et al. 1980; Prabhakara et al. 1981). Typical accuracies of 0.1 to 0.5 g cm^{-2} have been reported. The results obtained over land, however, have not been satisfactory, mainly because the surface emissivity in the microwave spectral region depends strongly on soil type and moisture. This strong and variable surface emission camouflages the water vapor information in the measurements.

Infrared measurements in the 6.3 μm rotation–vibration band from Nimbus-6, the NOAA series, GOES-5, and GOES-6 have been used to infer the vertical distribution of water vapor (e.g., Smith and Woolf 1976; Smith 1983), but with degraded accuracy, both in cloudy conditions and near the surface. The inversion techniques employed by these authors have typically yielded a 30% accuracy in the estimated water vapor mixing ratio.

It has long been observed, however, that direct solar radiation is absorbed substantially by water vapor in a cloudless atmosphere and that the phenomenon is even more pronounced when observations are conducted in the infrared part of the solar spectrum. Fowle (1912, 1913) was the first investigator to exploit these observations for measuring atmospheric water vapor amounts. He produced laboratory graphs relating the opacity of near-infrared water vapor bands to water vapor amount. His differential absorption concept has been subsequently verified and applied in many studies (e.g., Hand 1940; Foskett and Foster 1943; Gates 1956;

* Present affiliation: California Space Institute, Scripps Institution of Oceanography, La Jolla, California.

** Present affiliation: Laboratoire d'Etudes et de Recherches en Télédétection Spatiale, Toulouse, France.

Corresponding author address: Dr. Robert Frouin, California Space Institute, Scripps Institution of Oceanography, La Jolla, CA 92093-0221.

Siversten and Solheim 1975; Pitts et al. 1977; Reagan et al. 1987).

Fowle's concept is given further development in the present paper. We intend to demonstrate that it can be extended to the sensing of total water vapor amounts from space. For this purpose, we designed and constructed a radiometer that measures the intensity of the solar radiation reflected by the earth's surface in two spectral channels, one narrow, the other wide, centered on the absorption peak of the 940 nm water vapor band. The ratio of the radiometric signals measured by the two channels is independent of the surface reflectance properties and yields a direct estimate of the water vapor amount along the optical path. We report on the first few flights of this new device.

2. Differential absorption technique

The differential absorption technique consists of viewing a source of radiative energy at two (or more) wavelengths through the same atmospheric path; the wavelengths are chosen so that the absorption coefficients of a given gas, the amount of which is to be measured, are different. In the aforementioned investigations, the technique was applied to water vapor (the gas studied) by viewing the sun (the source) directly through the atmosphere. Instead of viewing the sun, however, one can view the earth's surface from above the atmosphere to estimate the water vapor amount along the optical path. In this case, it is the solar energy reflected by the surface that is measured, and this is done through a double atmospheric path (sun-to-surface and surface-to-sensor); but, a priori, one must know the surface reflectance. Here we derive a technique which requires no a priori knowledge of the surface reflectance.

We first consider the case of a direct path between the sun and the sensor. Denoting the voltage outputs of the radiometer in channels 1 and 2 by V_1 and V_2, we have the following proportionality:

$$\frac{V_1}{V_2} \sim \frac{I_1 \bar{t}_1}{I_2 \bar{t}_2} \tag{1}$$

where I_1 and I_2 are the source intensities and $\bar{t}_1$ and $\bar{t}_2$ are average transmission functions. If channel i ($i = 1, 2$) is characterized by the spectral response $R_i(\lambda)$, $\bar{t}_i$ is defined as

$$\bar{t}_i = \frac{\int_0^\infty t_i(\lambda) R_i(\lambda) d\lambda}{\int_0^\infty R_i(\lambda) d\lambda} \tag{2}$$

where λ is wavelength and $t_i(\lambda)$ is the spectral atmospheric transmittance. When the two channels are located in a spectral region where atmospheric absorption is essentially due to water vapor, $\bar{t}_1/\bar{t}_2$ can be expressed as a function of an equivalent amount of water vapor along the optical path, U^*. Measuring V_1/V_2, therefore, gives access to U^*.

We now consider a surface target illuminated by the sun. In this case, we have to account for the solar energy reflected by the target, which yields

$$\frac{V_1}{V_2} \sim \frac{I_1 \bar{r}_1 \bar{t}_1}{I_2 \bar{r}_2 \bar{t}_2} \tag{3}$$

where $\bar{r}_1$ and $\bar{r}_2$ are average target reflectances. If the channels are selected such that $\bar{r}_1/\bar{r}_2$ is a constant, V_1/V_2 remains a function of U^* only (I_1/I_2 does not depend on the type of atmosphere encountered), and we can still obtain U^* by measuring V_1/V_2.

In the present study, the technique employs two channels centered on practically the same wavelength at the absorption peak of the 940 nm water vapor band. The channels have narrow and wide spectral bandwidths, respectively. These characteristics, while differentiating between $\bar{t}_1$ and $\bar{t}_2$ for a fixed water vapor path, allow one to eliminate the ratio $\bar{r}_1/\bar{r}_2$ in (3) ($\bar{r}_1 \approx \bar{r}_2$). We are aware that the region around 940 nm is influenced not only by water vapor absorption, but also, although to a lesser degree, by carbon dioxide, ozone, and aerosol absorption as well as molecular and aerosol scattering. It is assumed, however, that the properties of all the attenuators except water vapor do not vary significantly (or vary linearly) across the channels' bandwidth and, thus, cancel in the ratio. This assumption is justified, as radiative transfer calculations performed with various standard atmospheres demonstrate (see section 3).

Note, furthermore, that (3) neglects the signal backscattered by the atmosphere toward the sensor, which may not be justified under certain atmospheric conditions (i.e., thick aerosol layers) when the surface reflectance is small. An analysis of this effect will be presented later in the paper, when examining the experimental results (section 5).

Let us now express the average atmospheric transmittance $\bar{t}_i$. For a homogenous path, two basic random band models can be used (for more details, see Paltridge and Platt 1976):

1) the model of Goody (1952)

$$\bar{t}_i \approx \exp\left[-\frac{\bar{S}_i U}{\bar{d}_i}\left(1 + \frac{\bar{S}_i U}{\pi \bar{\alpha}_i}\right)^{-1/2}\right]; \tag{4}$$

2) the model of Malkmus (1967)

$$\bar{t}_i \approx \exp\left\{-\frac{\pi \bar{\alpha}_i}{2\bar{d}_i}\left[\left(1 + \frac{4\bar{S}_i U}{\pi \bar{\alpha}_i}\right)^{1/2} - 1\right]\right\} \tag{5}$$

where $\bar{d}_i$ is the average line spacing, $\bar{\alpha}_i$ is the average Lorentz half-width, and $\bar{S}_i$ is the average line intensity. In these expressions it is assumed that the spectral interval considered is wide compared to $\bar{\alpha}_i$. Since $\bar{S}_i U$

$\gg \pi\bar{\alpha}_i$ in the water vapor bands above 0.7 μm, both (4) and (5) reduce to

$$\bar{t}_i \approx \exp\left[-\frac{(\bar{S}_i U \pi \bar{\alpha}_i)^{1/2}}{\bar{d}_i}\right]. \quad (6)$$

For a nonhomogenous path, the pressure and temperature variations along the path ($\bar{S}_i$ depends on temperature and $\bar{\alpha}_i$ depends on temperature and pressure) can be taken into account by scaling U appropriately. A one-parameter scaling approximation (e.g., Goody 1964) is sufficient, since the absorption regime is strong and the effect of tropospheric temperature changes on $\bar{S}_i$ is small. The scaled amount then takes the usual form:

$$U^* = \int_0^{U_t} \left(\frac{P}{P^*}\right)^m \left(\frac{T^*}{T}\right)^n dU \quad (7)$$

where T^* and P^* are the temperature and pressure of the equivalent homogenous path, respectively, and U_t is the water vapor amount integrated along the path. In the major water vapor absorption bands of the shortwave solar spectrum, including the 940 nm band, $m = 0.9$ to 1 and $n = 0.45$ (Selby et al. 1978; Stephens 1984). The procedure to calculate $\bar{t}_i$ is therefore to replace U with U^* in (6) and evaluate $\bar{S}_i$ at temperature T^* and $\bar{\alpha}_i$ at temperature T^* and pressure P^*.

Using the scaling approximation for a vertical atmospheric path characterized by a temperature profile $T = T_0 e^{-z/H_T}$, a pressure profile $P = P_0 e^{-z/H_P}$, and a water vapor density profile $\rho = \rho_0 e^{-z/H_W}$, and taking $T^* = T_0$ and $P^* = P_0$ yields

$$U^* = \rho_0 H_W \left(1 + \frac{mH_W}{H_P} - \frac{nH_W}{H_T}\right)^{-1}. \quad (8)$$

Typically, $H_T \approx 30$ km, $H_P \approx 8$ km, and $H_W \approx 2$ km, which gives:

$$U^* \approx 0.8\rho_0 H_W = 0.8 U_0 \quad (9)$$

where U_0 is the vertically integrated water vapor amount. Thus, U^* is relatively close to U_0. The factor relating U^* to U_0, however, is not constant and its changes result mainly from the variability of H_W (the effect of variations in H_T is negligible). Still, the relationship is stable enough to deduce accurately U_0 from U^*, as shown quantitatively in section 3.

The average transmittance $\bar{t}_i$ over a slant path can therefore be expressed as

$$\bar{t}_i \approx \exp[-\bar{\beta}_i (m^* U_0)^{1/2}] \quad (10)$$

where m^* is the equivalent air mass ($1/\cos\theta$ when viewing the sun at zenith angle θ and $1/\cos\theta + 1/\cos\theta'$ when viewing the surface at zenith angle θ' with the sun at zenith angle θ) and $\bar{\beta}_i$ is an average absorption coefficient. Note that atmospheric refraction cannot be neglected at high solar or viewing zenith angles (θ, $\theta' > 80°$). The resulting increase in air mass, however, can be easily taken into account using, for instance, Kasten's (1966) approximation formula.

Using (10), the ratio of atmospheric transmittances in the two channels takes the final form

$$\frac{\bar{t}_1}{\bar{t}_2} \approx \exp[-\bar{\beta}'(m^* U_0)^{1/2}] \quad (11)$$

where $\bar{\beta}' = \bar{\beta}_1 - \bar{\beta}_2$. By measuring $\bar{t}_1/\bar{t}_2$ and knowing $\bar{\beta}'$ and the radiation geometry, it is therefore possible, at least in principle, to derive U_0 from (11).

3. Radiometer

A schematic description of the radiometer is given in Fig. 1, and Table 1 lists the sensor specifications. The radiance passing through the collector is focused on one extremity of an optical fiber. Two condenser lenses form an image of the other extremity of the fiber on the detectors. Using fiber optics was appropriate because the instrument was designed to be flown on an aircraft. The detectors are silicon photodiodes operating at ambient temperature. Two interference filters are mounted in front of the detectors on a rotating wheel driven by a synchronous motor. The spectral response of the filters is shown in Fig. 2. The center wavelength is 938 nm for both filters, and their bandwidths are 13 and 46 nm at half-power points, respectively. These characteristics for the filters ensure that $\bar{r}_1/\bar{r}_2$ is practically equal to 1 in all conditions (surface type, illumination, and viewing geometry). Also shown in Fig. 2 is the spectral response of the detectors, which is fairly constant over the wavelength range of interest. The temperature dependence of the detector response is small, not exceeding 0.1% per degree Kelvin in the range of temperatures encountered in the troposphere. In addition to the filters, a reference surface is mounted to the wheel so that the detectors view an optically black target at each rotation of the wheel. A timing device permits control of the radiation signals generated by the optical system. The signals from the detectors are amplified and converted by a 12-bit analog-to-digital processor. Two amplifier sensitivities can be selected, and are appropriate for measurements over land (S_1) and sea (S_3), respectively. Once converted to digital format, the signals are fed into a data acquisition unit. The integration time is 0.05 s for each filter and the optical zero.

The differential technique requires only a relative calibration of the radiometric outputs. This calibration was carried out in the laboratory by directing the light collector toward a diffuse target illuminated by a solar simulator. The diffuse target was placed about 30 cm from the solar simulator and the light collector was installed just behind the diffuse target. Typical laboratory conditions were 292 K for air temperature and 80% for humidity. With this experimental setup and these conditions, atmospheric absorption along the optical path was negligible. The procedure was repeated

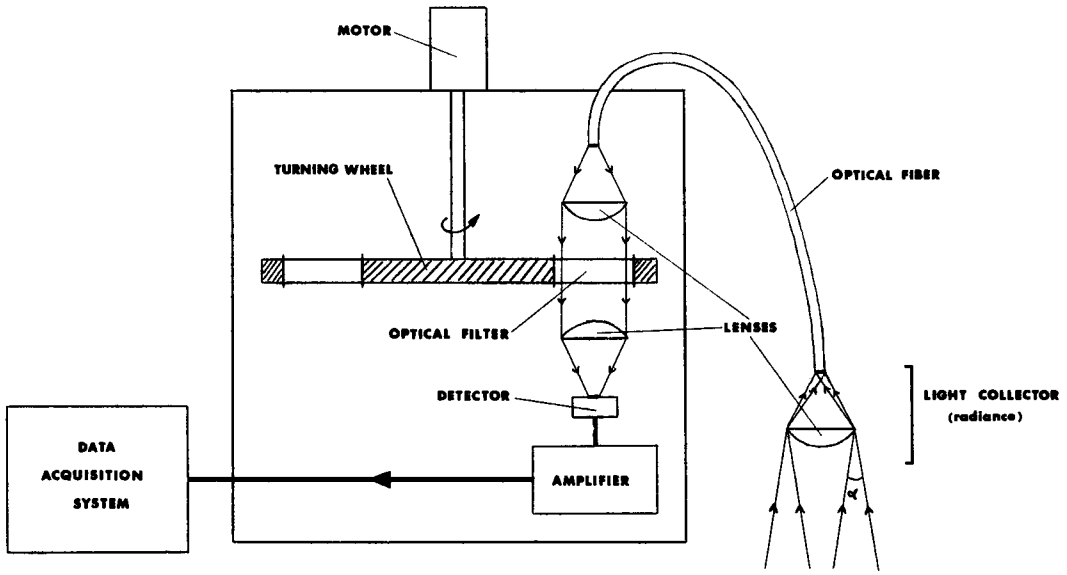

FIG. 1. Radiometer schematic description.

before and after each in situ experiment. The ratio V_1/V_2 was observed to vary little from one calibration to the next, by no more than a few tenths of a percent around the value 1/0.775.

Figure 3 gives the ratio of the transmission functions, $\bar{t}_1$ and $\bar{t}_2$, for the narrow and wide band channels, respectively, computed with the 5S code (Tanré et al. 1985, 1986) for different air masses and atmospheric conditions specified in the code. The salient features of the 5S code are given in the Appendix. In the calculations, the spectral atmospheric transmittance was convoluted with both the spectral response of the interference filters and the spectral response of the detectors. We see that $\bar{t}_1/\bar{t}_2$ fits fairly well with the law given by (11) and the coefficient $\tilde{\beta}'$ deduced from the simulation is 0.178 $g^{-1/2}$ cm. For a fixed water vapor amount, the dependence of $\bar{t}_1/\bar{t}_2$ on atmosphere type is negligible. The curve in Fig. 3, which was obtained

TABLE 1. Radiometer characteristics.

Parameter	Value/description
	Design Parameters
Wavelength at half-power points	927–944 nm (narrow), 914–959 nm (wide)
Instantaneous field-of-view (total)	3° (instrument viewing the sun); 11.5° (instrument viewing the surface)
Collecting aperture diameter	3 cm
Rotating wheel (supporting the optical filter)	3 positions (2 filters + a zero); 2 rps
Detector type	photodiodes EG&G (type: HUV 4000)
Detector operating temperature	ambient
Amplifier sensitivity	S_1: 0.12 W m^{-2} sr^{-1}/V; S_3: 0.46 W m^{-2} sr^{-1}/V
Dynamic range	
Narrow-band channel	0–0.49 W m^{-2} sr^{-1}
Broad-band channel	0–1.84 W m^{-2} sr^{-1}
Integration time	0.05 s
Cadence of measurements	1 measurement (2 filters + zero) every 0.5 s
Signal quantizing levels	4096 (12-bit coding)
	Noise equivalent radiance
Narrow-band channel	S_1: 0.12×10^{-3} W m^{-2} sr^{-1}; S_3: 0.42×10^{-3} W m^{-2} sr^{-1}
Broad-band channel	S_1: 0.46×10^{-3} W m^{-2} sr^{-1}; S_3: 1.61×10^{-3} W m^{-2} sr^{-1}
	Physical characteristics
Weight	4 kg
Size	20 × 20 × 24 cm
Power (high/low)	70/25 W

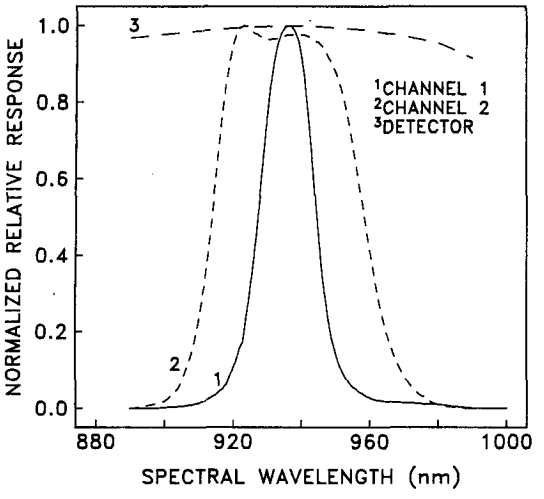

FIG. 2. Spectral response of the interference filters and detectors.

by least-square fitting $\log(\bar{t}_1/\bar{t}_2)$ as a function of $(m^*U_0)^{1/2}$, departs significantly from the simulated points at water vapor amounts above 15 g cm^{-2}. At m^*U_0 = 17 g cm^{-2}, for instance, the discrepancy in $\bar{t}_1/\bar{t}_2$ reaches 0.014, which translates into a 10% error on m^*U_0. Small solar and viewing zenith angles are therefore favored for greater accuracy in the water vapor retrievals. Note also that the radiometer is sufficiently sensitive to $\bar{t}_1/\bar{t}_2$ variations in the 0–20 g cm^{-2} range of water vapor amounts considered in Fig. 3: V_1/V_2 and, hence, $\bar{t}_1/\bar{t}_2$, are measured to within a few thousandths.

4. Measurements

a. Ground-based measurements

The two-channel radiometer was used in a sun-viewing configuration from the ground to validate (11) and derive experimentally the coefficient $\bar{\beta}'$. Measurements were made at several locations and various dates in France and Niger: Dinard (48.38°N, 2.03°W) on 20 June 1980; Lille (50.39°N, 3.05°E) on 13 and 15 May 1980; Roscoff (48.43°N, 3.59°W) on 16 September 1980; and Niamey (13.32°N, 2.05°E) on 19, 20, 21, 23, 24, 26, and 29 November and 1, 2, 3, 4, 5, and 7 December 1980. For each day, the data were collected at regular time intervals when $\theta < 80°$ ($1 < m^* < 5$). Radiosonde observations were available for Niamey (one launch per day at 1200 UTC), but not for the other locations. In order to estimate U_0 at those locations, we used 0000 and 1200 UTC radiosonde observations at the nearest launch sites, namely Brest (48.45°N, 4.41°W), Trappes (48.76°N, 2.01°E), and Camborne (50.21°N, 5.31°W) for Dinard and Roscoff, and Uccle (50.80°N, 4.35°E), Crawley (51.08°N, 0.21°W), and Trappes for Lille, and weight-averaged the computed total water vapor amounts according to distance between the radiosondes and the radiometer. Time differences between radiometer measurements and radiosonde launches were accounted for by linearly interpolating the radiosonde data. The above-described procedure is indeed subject to error, especially since some of the radiosonde sites were located several hundreds of kilometers from the experiment sites. Most of the radiometer data, however, were acquired in Niamey, where radiosondes are launched on a regular basis. Processing the radiosonde data revealed that total water vapor amounts ranged from 1 to 2 g cm^{-2}. This range of U_0 values is small (in a tropical atmosphere, U_0 can exceed 4 g cm^{-2}), but according to theory, $\bar{t}_1/\bar{t}_2$ is governed by m^*U_0 and not atmosphere type (see Fig. 3). Therefore, calibrating the instrument in the range 1–2 g cm^{-2} for U_0 (using m^* from 1 to 5) should also be valid for $U_0 > 2$ g cm^{-2}.

Figure 4 shows the ratio of the intercalibrated signals generated in the narrow and wide spectral channels as a function of m^*U_0, from which $\bar{\beta}'$ can be deduced by regression. This was done as for the simulations in Fig. 3. Table 2 gives the values of $\bar{\beta}'$ obtained for each day of measurements. The overall mean value of $\bar{\beta}'$ is 0.185 $\pm$ 0.14 (1σ) g$^{-1/2}$ cm. The dispersion of $\bar{\beta}'$, 7.5% (1σ) of the mean value, is due largely to uncertainties in the radiosonde total water vapor amounts [10%–15% errors are frequently reported; for instance, see Richner and Phillips (1982)]. Also, the mean value of $\bar{\beta}'$ corresponds fairly well to the value predicted by the 5S code (0.178 g$^{-1/2}$ cm) within the accuracy of this code and experimental uncertainties. We conclude that the two-channel radiometer may derive total water vapor amount with a 15% (1σ) accuracy (a 7.5% uncertainty on $\bar{\beta}'$ yields at 15% uncertainty on m^*U_0) using (11),

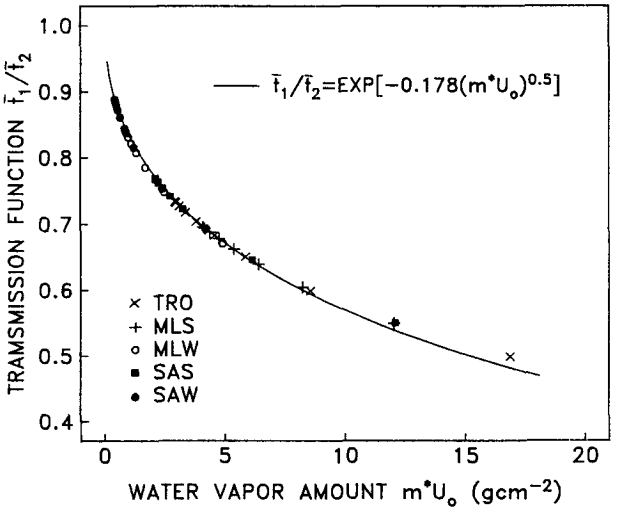

FIG. 3. 5S simulations of the transmission function $\bar{t}_1/\bar{t}_2$ for different water vapor amounts and atmosphere types (tropical, midlatitude summer, midlatitude winter, subarctic summer, subarctic winter).

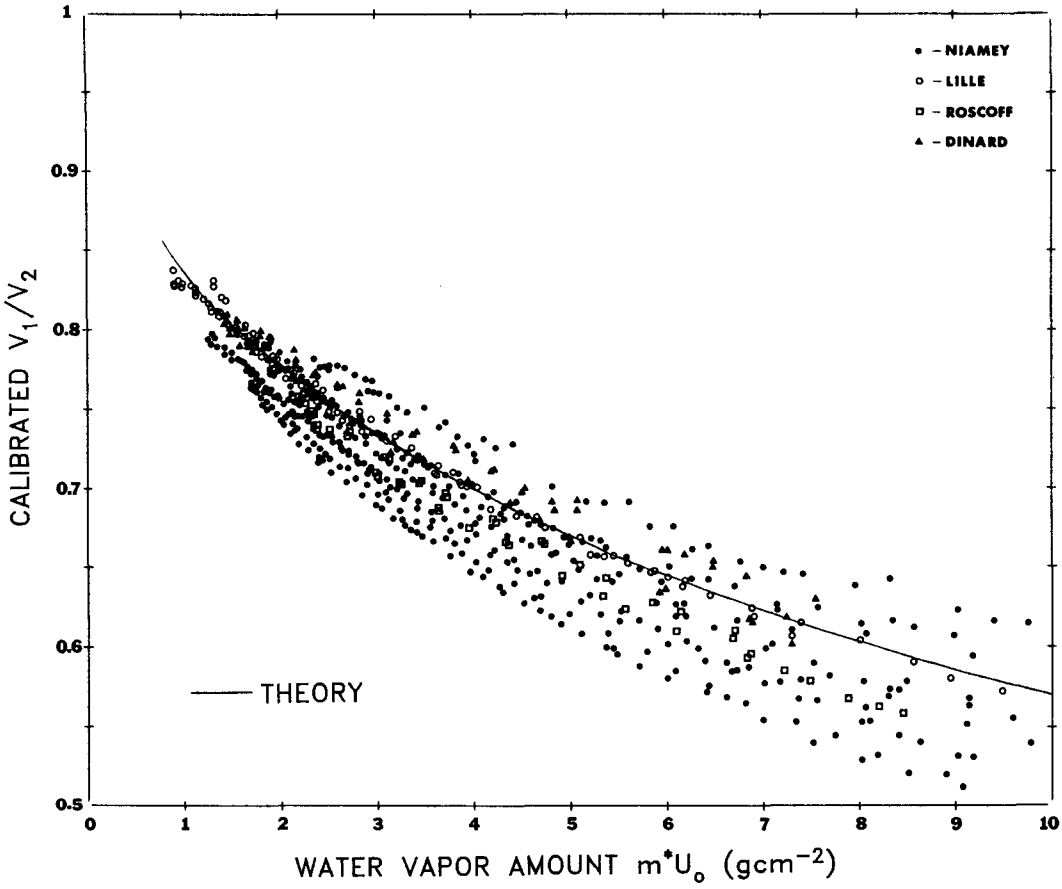

FIG. 4. Ground-based measurements in Lille, Dinard, Roscoff, and Niamey (radiometer viewing the sun): calibrated ratio of voltage outputs V_1 and V_2 as a function of water vapor amount m^*U_0.

with $\bar{\beta}'$ empirically fitted as 0.185 $g^{-1/2}$ cm. It is important to emphasize, however, that the 15% accuracy indicated above corresponds to one standard deviation in $\bar{\beta}'$ and is therefore valid at the 68% confidence level if we assume a normal distribution of m^*U_0 values for any V_1/V_2 measurement.

b. Airborne measurements

In order to demonstrate the validity of deriving total water vapor amounts from space by measuring the solar radiation reflected by the Earth's surface, we installed the two-channel radiometer aboard a small aircraft with the light collector viewing the Earth's surface at nadir. Two flights were made on 16 May 1979 and 22 May 1980 over sea and land in the northern part of France. Figure 5 shows the aircraft flight pattern for each day as well as the nearest radiosonde launch sites (Uccle, Trappes, and Crawley), and Table 3 displays the total water vapor amounts at these sites before and after the flights. The aircraft flew over varied surfaces (forest, crops, bare soil, and ocean) whose altitudes did not exceed 100 m above mean sea level.

Figures 6a, 6b, and 6c present the data acquired during the flight of 16 May 1979 at 2800 m altitude over land. The two channels' voltage outputs are plotted as a function of time in Figs. 6a and 6b, respectively, and their calibrated ratio is shown in Fig. 6c. It is striking that each channel output varies rapidly with time, echoing changes in the surface reflectance, while the ratio of these outputs is very independent of the surface properties. This proves quite well that using two channels centered on the same wavelength allows one to eliminate surface reflectance effects. The ratio in Fig. 6c, however, exhibits a few abnormal values. Due to a malfunction of the timing device, the measurement in the narrow band channel was erratically skipped. The problem was corrected prior to the second flight on 22 May 1980.

Figures 7a, 7b, and 7c show the data record for 22 May 1980 when flying at 900 m altitude over land and sea. Again the ratio of the two voltage outputs (Fig. 6c) is quite independent of the surface properties, even when passing from land to sea, and the technique also worked when measuring the small radiation energy reflected by the sea surface.

TABLE 2. Best linear fit between calibrated V_1/V_2 and $\exp[-\beta' \times (m^*U_0)^{1/2}]$ for the different ground-based measurements (instrument viewing the sun). The mean $\bar{\beta}'$ value is 0.185 ± 0.014 g$^{-1/2}$ cm.

Location	Date (d/mo/yr)	$\bar{\beta}'$ (g$^{-1/2}$ cm)	Residual error
Dirard, France (48.38°N, 2.03°W)	22/6/80	0.175	0.008
Lille, France (50.39°N, 3.05°E)	13/5/80	0.117	0.009
	15/5/80	0.165	0.009
Roscoff, France (48.43°N, 3.59°W)	17/9/80	0.189	0.005
Niamey, Niger (13.32°N, 2.05°E)	19/11/80	0.174	0.015
	20/11/80	0.167	0.018
	21/11/80	0.207	0.020
	23/11/80	0.174	0.013
	24/11/80	0.184	0.012
	26/11/80	0.176	0.009
	29/11/80	0.207	0.006
	01/12/80	0.210	0.003
	02/12/80	0.182	0.010
	03/12/80	0.194	0.002
	04/12/80	0.202	0.002
	05/12/80	0.194	0.001
	07/12/80	0.175	0.003

When flying at such relatively low altitudes, the water vapor amount along the optical path is not m^*U_0, with m^* defined in section 2, but

$$U_e = U_0/\cos\theta + U'_0/\cos\theta' \qquad (12)$$

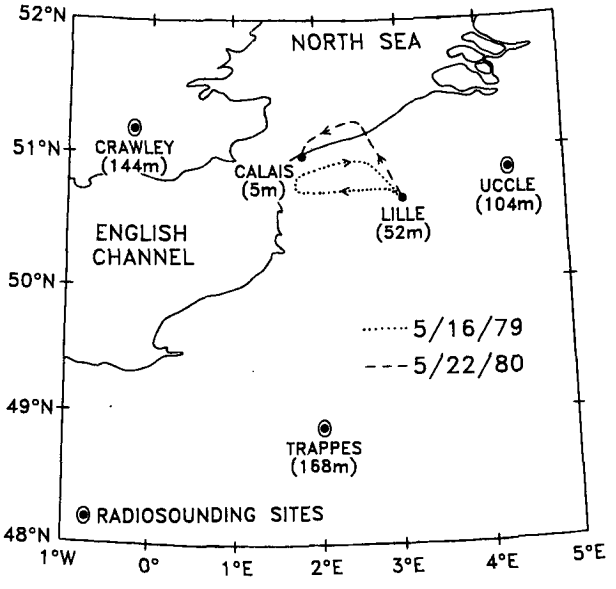

FIG. 5. Aircraft flight pattern for 16 May 1979 and 22 May 1980. The nearest radiosonde launch sites are also shown.

TABLE 3. Radiosonde data used to compute total water vapor amounts along the aircraft flight paths.

Station	Date (d/mo/yr)	Time (UTC)	Water vapor amount U_0 (g cm^{-2})
Crawley	16/5/79	00	2.01
	16/5/79	12	1.94
	22/5/80	00	1.78
	22/5/80	12	1.77
Trappes	16/5/79	00	1.96
	16/5/79	12	1.89
	22/5/80	00	2.27
	22/5/80	12	1.95
Uccle	16/5/79	00	1.87
	16/5/79	12	2.46
	22/5/80	00	2.05
	22/5/80	12	1.78

where U'_0 is the water vapor amount along the path from the surface to the flying altitude. Figures 8a and 8b give U_e as a function of time for each flight, deduced from the radiometer measurements and computed from radiosonde observations. The radiosonde data were weight-averaged according to the distance between the launch sites and the aircraft location during the flights, taking into account differences between the altitude of the launch sites and the altitude of the surface viewed by the radiometer. The procedure was performed for times preceding and following the flights, and the resulting water vapor amounts were interpolated linearly with time. As seen in the figures, the agreement between the two types of U_e estimates is fairly good. For the flight of 16 May 1979 (Fig. 8a), the average value of U_e obtained by the differential method is 5.2 g cm^{-2}, and compares with 4.5 g cm^{-2} from the radiosonde data. For the flight of 22 May 1980 (Fig. 8b), the values are 2.2 and 2.6 g cm^{-2}, respectively. These results, however, are not conclusive; they are based on only two flights. Furthermore, uncertainties in the water vapor amounts derived from the radiosonde data may be largely responsible for the discrepancies. A definitive assessment of the method will require more measurements. Perhaps an optimum means of verification would be to install the instrument aboard a helicopter flying above the planetary boundary layer (where most of the water vapor is concentrated) and over surface areas where concurrent high-quality radiosonde observations are made as well as standard sunphotometer measurements.

5. Aerosol contribution to measurement errors

A possible limitation of the method over the ocean should be pointed out. At the very low level of the radiation signal reflected by the sea surface, the aerosol scattering contribution cannot be ignored and may lead to an underestimation of the water vapor amount. Let us assume, for the sake of simplification, that the sur-

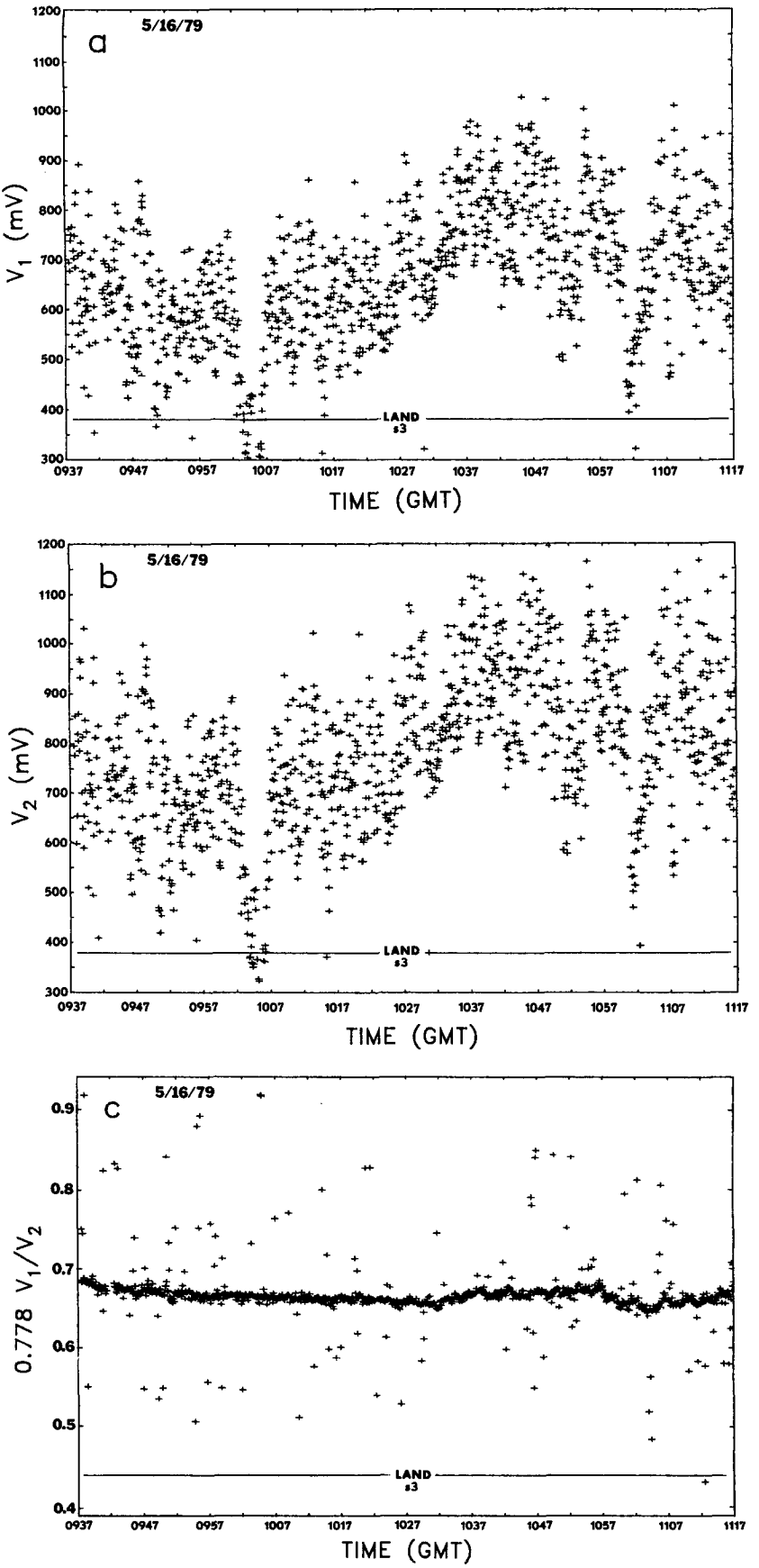

FIG. 6. Flight of 16 May 1979 at 2800 m MSL altitude over land (radiometer viewing the surface): time evolution of the voltage outputs V_1 (a), V_2, (b), and of their calibrated ratio (c).

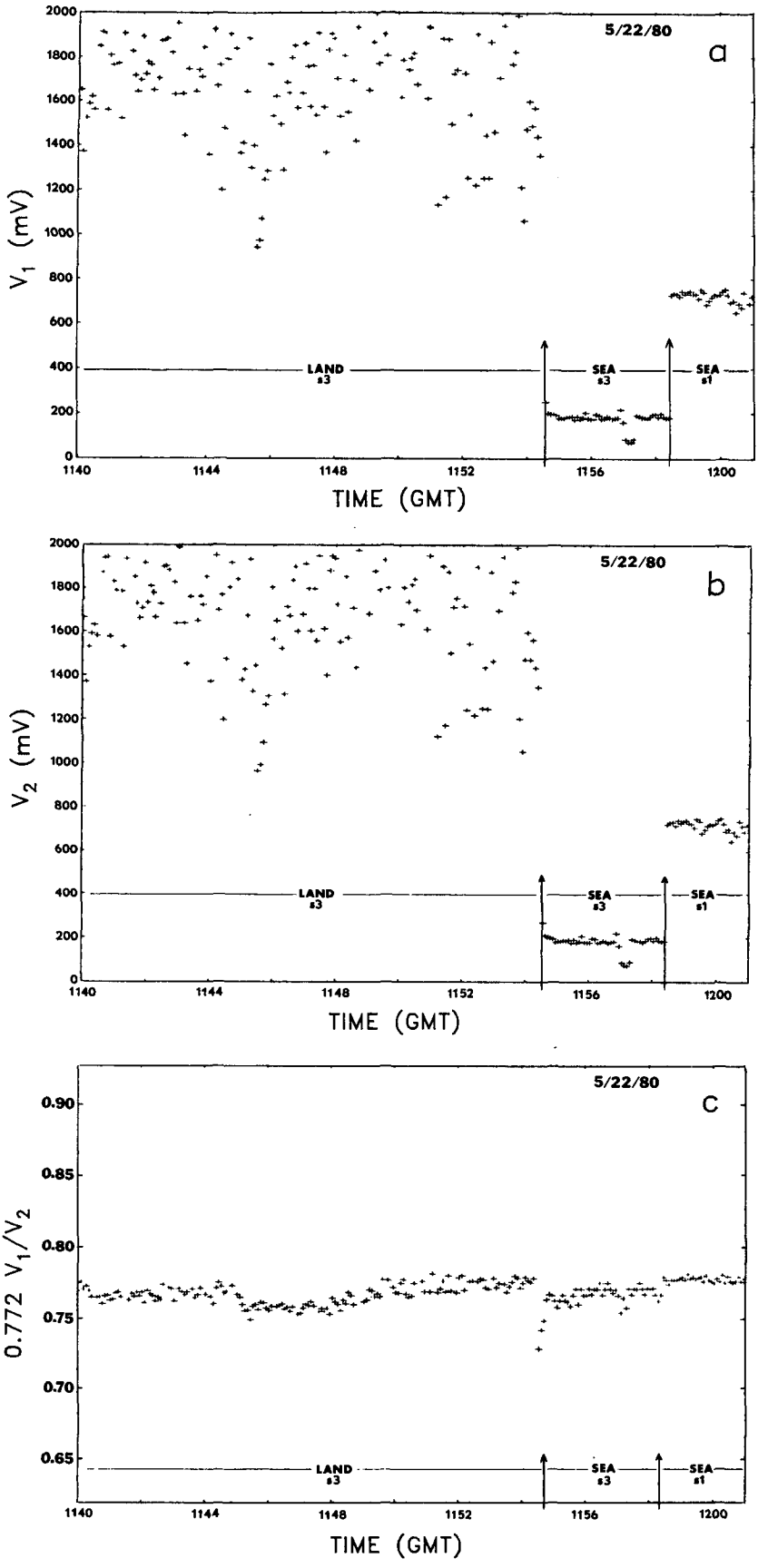

FIG. 7. As in Fig. 5, but for the flight of 22 May 1980 at 900 m MSL altitude over land and sea.

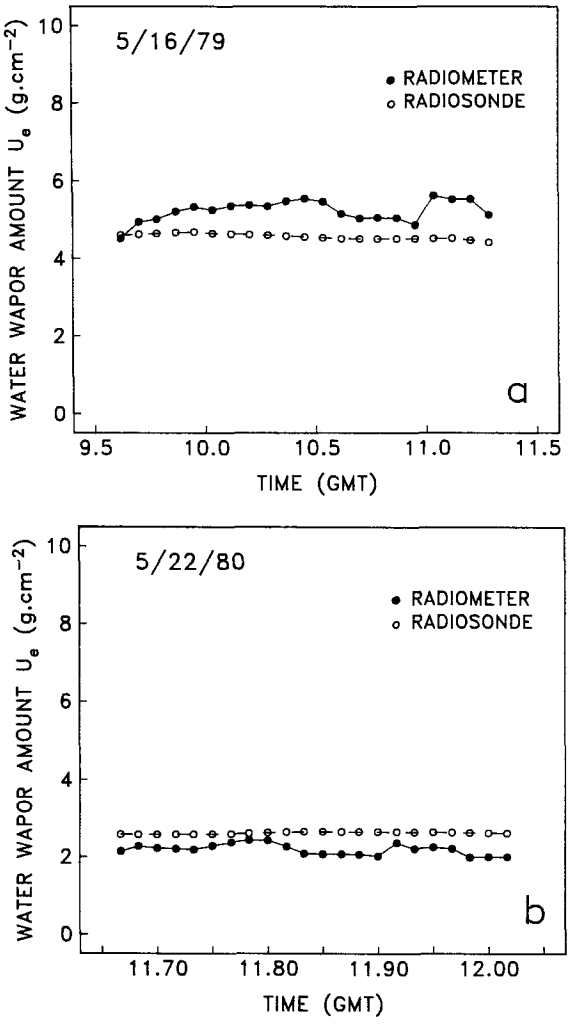

FIG. 8. Time evolution of retrieved and observed water vapor amounts for the flights of (a) 16 May 1979 and (b) 22 May 1980.

face reflectance is null and that the diffuse atmosphere is composed only of aerosols whose concentration decreases exponentially with altitude (optical thickness τ_A, scattering phase function P_A, single scattering albedo ω_{0A}, scale height H_A). Let us further assume that the aerosol optical properties vary smoothly with wavelength, so that they can be considered equal in the narrow and wide spectral channels. Using the first order scattering approximation, the aerosol atmosphere scatters toward the sensor in channel i the radiance (e.g., Deschamps et al. 1983):

$$L_i = \omega_{0A} \frac{P_A}{4\cos\theta'} \frac{I_i}{\pi} \int_0^\infty \bar{t}_i(z, \infty) \frac{d\tau_A(z)}{dz} dz. \quad (13)$$

In this expression, $\bar{t}_i(z, \infty)$ and $d\tau_A(z)/dz$ can be written:

$$\bar{t}_i(z, \infty) \approx \exp\{-\bar{\beta}_i[m^*U(z, \infty)]^{1/2}\} \quad (14)$$

$$\frac{d\tau_A(z)}{dz} = -\frac{\tau_A}{H_A} \exp\left(-\frac{z}{H_A}\right) \quad (15)$$

where $U(z, \infty)$ is the vertically integrated water vapor amount between altitude z and the top of the atmosphere.

Developing the right-hand side of (14) to first order in $U(z, \infty)$ and taking $U(z, \infty) = U_0 \exp(-z/H_W)$ yields

$$\bar{t}_i(z, \infty) \approx 1 - \bar{\beta}_i(m^*U_0)^{1/2} \exp\left(-\frac{z}{2H_W}\right). \quad (16)$$

Although this approximation for $\bar{t}_i(z, \infty)$ is not verified (by definition, water vapor absorption is strong in the 940 nm band), it is sufficient to provide the order of magnitude of the aerosol backscattering effect on the differential method's accuracy.

Substituting (15) and (16) into (13), one can easily evaluate the integral on the right-hand side of (13), which gives

$$L_i \approx \omega_{0A} \frac{P_A\tau_A}{4\cos\theta'} \frac{I_i}{\pi} \times \left[1 - \bar{\beta}_i(m^*U_0)^{1/2}\left(\frac{2H_W}{H_A + 2H_W}\right)\right]. \quad (17)$$

Since the ratio of the radiometer voltage outputs in the narrow and wide spectral channels is proportional to L_1/L_2, we have

$$\frac{V_1}{V_2} \sim \frac{I_1}{I_2} \frac{1 - \bar{\beta}_1\left[m^*U_0\left(\frac{2H_W}{H_A + 2H_W}\right)^2\right]^{1/2}}{1 - \bar{\beta}_2\left[m^*U_0\left(\frac{2H_W}{H_A + 2H_W}\right)^2\right]^{1/2}}. \quad (18)$$

Thus, the total water vapor amount detected is

$$U_{0a} \approx U_0\left(\frac{2H_W}{H_A + 2H_W}\right)^2. \quad (19)$$

Taking typical values of 0.5 km (e.g., Patterson et al. 1980) and 2 km (e.g., Roll 1965) for H_A and H_W, respectively, over the ocean, we obtain $U_{0a} \approx 0.79U_0$, which indicates that the retrieved total water vapor amount is underestimated by 21%. If H_A is higher or $H_A \approx H_W$, the error becomes unacceptable. One has to point out, however, that (19) gives a superior error limit. As soon as the surface reflectance reaches a few percent, the contribution to L_i of photons reflected by the surface generally surpasses that of photons uniquely backscattered by the atmosphere.

In fact, no noticeable decrease in U_e is observed on 22 May 1980 when passing from land to sea around 11.9 UTC (Fig. 8b). On the contrary, U_e increased from 2.0 to 2.3 g cm^{-2}. This change may be attributed to the amplifier sensitivity S_3 used over land, which is not adapted to measurement over the ocean. After

switching to the more appropriate sensitivity S_1, U_e quickly recovered the value of 2.0 g cm^{-2} observed over land.

6. Summary and concluding remarks

From the ground-based measurements, we have first shown that the differential technique can be used to derive total water vapor amounts by viewing the sun through the atmosphere in two channels of different spectral bandwidths centered on the same wavelength near 940 nm. The experiment was calibrated by comparing the ratio of the radiometric outputs generated for the two channels with water vapor amounts deduced from radiosonde observations. The relative accuracy of the water vapor retrievals is 15% (1σ). This value, however, incorporates uncertainties in the radiosonde data (including space and time interpolation errors), so that the actual accuracy is likely to be better, probably around 5%.

The two-channel radiometer was then used in an airborne configuration, measuring the solar radiation reflected by the Earth's surface. In this configuration, the instrument was able to yield a measure of the water vapor amount along the optical path independent of the surface nature, even for the lower radiation signals reflected by the sea surface. In the presence of thick aerosol layers, however, the water vapor amounts derived over the ocean may be underestimated by as much as 20%. One way to remove this limitation, at least partially, is to view the sea surface in the sun glint, which substantially increases the contribution of the signal reflected by the sea surface. Additionally, viewing the sea surface inside and outside the sunglint region would provide information on the ratio of aerosol and water vapor scale heights by giving access to U_0 and U_{0a} [see Eq. (19)].

We conclude by suggesting that the differential absorption technique presented herein can be applied to yield accurate space observations of total water vapor amounts under clear sky conditions over land and sea. Compared to satellite microwave techniques, which are preferred over the ocean since they are applicable in almost all weather conditions, our technique has the advantage of simplicity and would complement the microwave techniques over land where they fail. Interestingly, the Earth Observing System of the 1990s will carry the High Resolution Imaging Spectrometer (HIRIS), an instrument that possesses adequate channels to exploit our differential absorption concept.

Acknowledgments. This work was supported by the Centre National d'Etudes Spatiales, the Centre National de la Recherche Scientifique, and the California Space Institute. The authors gratefully acknowledge C. Verwaerde for realizing the electronics of the radiometer, J. Y. Balois for his help in taking the measurements, C. Deroo for her programming support, B. Bloomfield for editing suggestions, and R. Markworth for typing the manuscript. One of us, R. Frouin, who piloted the plane during the field experiments, wishes to thank E. Maes for his assistance in pre- and postflight operations at the Lille–Bondues airport.

APPENDIX

The 5S Code

The Simulation of the Satellite Signal in the Solar Spectrum (5S) code (Tanré et al. 1985, 1986) computes the solar radiation backscattered to space by the Earth–atmosphere system as it may be observed by a satellite sensor. Given a Lambertian ground target, the code estimates the target's apparent reflectance by taking into account the effects of gaseous absorption, scattering by molecules and aerosols, and spatial inhomogeneities in the surface reflectance. The input parameters, namely, solar and viewing geometries, atmosphere model, surface reflectance, and spectral band, can either be specified from standard conditions or user-defined. In addition to apparent reflectance, the code provides gaseous transmittance and irradiance at the surface, as well as the various components of the satellite signal. Complementary results are also available; exact calculations at selected wavelengths, in particular, allow one to assess the code accuracy.

Based on Tanré et al. (1979), the satellite signal is expressed as a function of the successive orders of radiation interactions in the coupled surface–atmosphere system. If ρ is the reflectance of the target, and ρ_e that of its environment, the apparent reflectance is written as

$$\rho^*(\theta, \theta', \phi) = t_g(\theta, \theta')\left\{\rho_a(\theta, \theta', \phi) + \frac{[e^{-\tau/\cos\theta} + t_d(\theta)]}{1 - \rho_e S}[\rho e^{-\tau/\cos\theta'} + \rho_e t_d(\theta')]\right\} \quad \text{(A1)}$$

where θ and θ' are the sun and satellite zenith angles, respectively, ϕ the relative azimuth between sun and satellite directions, τ the atmospheric optical thickness, t_g the gaseous transmittance, t_d the atmospheric diffuse transmittance, and S the spherical albedo of the atmosphere. The first term enclosed by the curly brackets represents the contribution of photons backscattered to space without surface reflection, whereas the second term characterizes photons that have sustained one or multiple surface reflections. Absorption by atmospheric gases is considered as a single multiplicative factor dependent on the direct paths sun-to-surface and surface-to-sensor. Decoupling absorption and scattering processes are justified since, on the one hand, ozone is located at altitudes where molecules are rarefied, and on the other, water vapor and carbon dioxide absorption occur above 850 nm where molecular scattering is negligible, and first and second orders of aerosol scattering (predominantly forward) restitute almost all

of the diffuse radiation. According to Tanré et al. (1986), the error introduced by separating the two processes is smaller than one percent, except for grazing incidence or observation directions ($\cos\theta, \cos\theta' < 0.1$).

The atmospheric functions t_d and S are approximated by analytical formulas determined empirically from exact radiative transfer computations performed for a wide range of model atmospheres. Table A1 shows the disparity between 5S and exact calculations of the total atmospheric diffuse transmittance, $e^{-\tau/\cos\theta} + t_d(\theta)$, for various solar zenith angles and wavelengths. Calculations were made for two atmospheres, clear and hazy. The differences are small, generally less than 1%, but may reach over 2% (hazy atmosphere, $\theta = 60°$).

The gaseous transmittance, t_g, is computed from two exponential random band models, that of Goody (1964) for water vapor, and of Malkmus (1967) for oxygen, ozone, and carbon dioxide. The spectral resolution, 20 cm^{-1}, is sufficient (contains enough spectral lines) to apply the random band models confidently. Figure A1 compares the gaseous transmittance in the spectral region of the 940 nm water vapor band computed using the 5S code and with a well-known code, LOWTRAN-6 (Kneizys et al. 1983). For the tropical and midlatitude summer atmospheres considered, the agreement is good near the peak water of vapor absorption, but notable differences exist in the wings of the band. We recall here that for computational efficiency, LOWTRAN-6, unlike 5S, neglects the influence of temperature on the molecular absorption coefficient, and approximates molecular line absorption by a one parameter band model. Nevertheless, integration over the wavelength range of the narrow and wide bandpasses considered in the present study provides very similar results with both codes.

TABLE A-1. Comparison between 5S and exact calculations of the total atmospheric diffuse transmittance.

	$\theta = 15°$		$\theta = 60°$	
Wavelength (nm)	5S	Exact	5S	Exact
	Clear atmosphere			
450	.877	.873	.755	.753
550	.930	.928	.841	.839
650	.954	.953	.885	.883
850	.973	.973	.926	.924
1600	.988	.989	.966	.963
2200	.992	.993	.976	.975
	Hazy atmosphere			
450	.810	.806	.648	.633
550	.866	.864	.721	.705
650	.895	.895	.766	.750
850	.926	.927	.819	.806
1600	.963	.964	.899	.890
2200	.973	.976	.925	.921

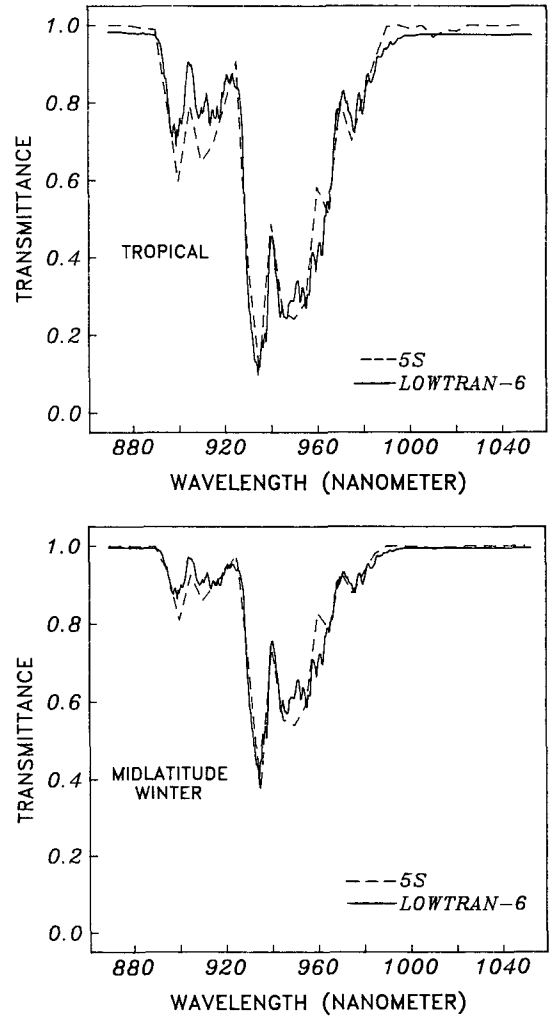

FIG. A-1. Gaseous transmittance along a vertical path sun-to-surface computed with 5S and LOWTRAN-6 for tropical and midlatitude winter atmospheres.

REFERENCES

Chang, A. T. C., and T. T. Wilheit, 1979: Remote sensing of atmospheric water vapor, liquid water and wind speed at the ocean surface by passive microwave techniques from the NIMBUS-5 satellite. *Radio Sci.*, **14**, 793–803.

Deschamps, P. Y., M. Herman, and D. Tanré, 1983: Modélisation du rayonnement réfléchi par l'atmosphere et la terre, entre 0,35 et 4 μm. ESA Rep. 4393/80/F/DD(SC), Eur. Space Agency, 165 pp..

Foskett, L. W., and N. B. Foster, 1943: A spectroscopic hygrometer. *Bull. Amer. Meteor. Soc.*, **24**, 146–153.

Fowle, F. E., 1912: The spectroscopic determination of aqueous vapor. *Astrophys. J.*, **35**, 149–162.

——, 1913: The determination of aqueous vapor above Mount Wilson. *Astrophys. J.*, **37**, 359–372.

Gates, D. M., 1956: Infrared determination of precipitable water in a vertical column of the earth's atmosphere. *J. Meteor.*, **13**, 369–375.

Goody, R. M., 1952: A statistical model for water vapour absorption. *Quart. J. Roy. Meteor. Soc.*, **78**, 165–169.

——, 1964: *Atmospheric Radiation, I: Theoretical Basis.* Clarendon Press, 436 pp.

Grody, N. C., A. Gruber and W. C. Shen, 1980: Atmospheric water content over the tropical Pacific derived from the NIMBUS-6 scanning microwave spectrometer. *J. Appl. Meteor.*, **19,** 986–996.

Hand, J. F., 1940: An instrument for the spectroscopic determination of precipitable atmospheric water vapor and its calibration. *Mon. Wea. Rev.*, **68,** 95–98.

Kasten, F., 1966: A new table and approximation formula for the relative optical air mass. *Arch. Meteor. Geophys. Bioklimatol.*, **B14,** 206–223.

Kneizys, F. X., E. P. Shettle, W. O. Gallery, J. H. Chetwynd, Jr., L. W. Abreu, J. E. A. Selby, S. A. Clough and R. W. Fenn, 1983: Atmospheric transmittance/radiance: computer code LOWTRAN 6. Envir. Res. Pap. No. 846, AFGL-TR-83-0187, Hanscom AFB, Massachusetts, 200 pp.

Malkmus, W., 1967: Random Lorentz band model with exponential-tailed S-1 line intensity. *J. Opt. Soc. Am.*, **57,** 323–329.

Paltridge, G. W., and C. M. R. Platt, 1976: *Radiative Processes in Meteorology and Climatology.* Elsevier Scientific, 318 pp.

Patterson, E. M., C. S. Kiang, A. C. Delany, A. F. Wartenburg, A. C. D. Leslie and B. J. Huebert, 1980: Global measurements of aerosols in remote continental and marine regions: Concentrations, size distributions, and optical properties. *J. Geophys. Res.*, **85,** 7361–7376.

Pitts, D. E., W. E. McCallum, M. Heidt, K. Jeske, J. T. Lee, D. De Monbrun, A. Morgan and J. Potter, 1977: Temporal variations in atmospheric water vapor and aerosol optical depth determined by remote sensing. *J. Appl. Meteor.*, **16,** 1312–1321.

Prabhakara, C., D. Chang and T. C. Chang, 1981: Remote sensing of precipitable water over the oceans from NIMBUS-7 microwave measurements. *J. Appl. Meteor.*, **21,** 59–68.

Reagan, J. A., K. Thome, B. Herman and R. Gall, 1987: Water vapor measurements in the 0.94 minor absorption band: calibration, measurements, and data applications. *Proceedings of IGARSS 87 Symposium, Ann Arbor, Michigan,* 63–67.

Richner, H., and P. D. Phillips, 1982: The radiosonde intercomparison: SONDEX, Spring 1981, Payerne. *Pure Appl. Geophys.*, **120,** 852–1198.

Roll, H. U., 1965: *Physics of the Marine Atmosphere.* Academic Press, 426 pp.

Selby, J. E. A., F. X. Kneizys, J. H. Chetwynd and R. A. McClatchey, 1978: Atmospheric transmittance/radiance computer code LOWTRAN-4. AFGL-TR-0053 Envir. Res. Paper No. 587, 79 pp.

Siversten, S., and J. F. Solheim, 1975: A field instrument for water vapor measurements. *Infrared Phys.*, **15,** 79–82.

Smith, W. L., 1983: The retrieval of atmospheric profiles from VAS geostationary radiance observations. *J. Atmos. Sci.*, **40,** 2025–2035.

——, and H. M. Woolf, 1976: The use of eigenvectors of statistical covariance matrices for interpreting satellite sounding radiometer observations. *J. Atmos. Sci.*, **33,** 1127–1140.

Staelin, D. H., W. H. Ledsham, R. L. Pettyjohn, P. W. Rosenkranz, R. K. L. Poon and J. W. Waters, 1976: Microwave sensing of atmospheric temperature and humidity from satellites. *Space Research XVI,* M. J. Rycroft, Ed., Akademie-Verlag.

Stephens, G. L., 1984: A review of the parameterizations of radiation for numerical weather prediction. *Mon. Wea. Rev.*, **112,** 826–867.

Tanré, D., M. Herman, P. Y. Deschamps and A. Deleffe, 1979: Atmospheric modeling for measurements of ground reflectances, including bidirectional properties. *Appl. Opt.*, **18,** 3587–3596.

——, C. Deroo, P. Duhaut, M. Herman, J. J. Morcrette, J. Perbos and P. Y. Deschamps, 1985: Effets atmospheriques en teledetection-logiciel de simulation du signal satellitaire dans le spectre solaire. *Proc. Third Int. Colloq. on Spectral Signatures of Objects in Remote Sensing, Les Arcs, France,* 315–319.

——, ——, ——, ——, ——, ——, and ——, 1986: Simulation of the Satellite Signal in the Solar Spectrum (5S). Internal Report, Laboratoire d'Optique Atmosphérique, Université de Lille, France, 267 pp.